

Exhumation history of a section of the Sikkim Himalayas, India: records in the metamorphic mineral equilibria and compositional zoning of garnet

Jibamitra Ganguly^{a,*}, Somnath Dasgupta^b, Weiji Cheng^a, Sudipta Neogi^c

^a Department of Geosciences, University of Arizona, Tucson, AZ 85721, USA

^b Department of Geological Sciences, Jadavpur University, Calcutta 700 032, India

^c Geological Survey of India, Petrology Division, Eastern Region, 15 Kyd Street, Calcutta 700 016, India

Received 31 January 2000; received in revised form 22 September 2000; accepted 25 September 2000

Abstract

The exhumation history of pelitic migmatite samples from the High Himalayan Crystalline Complex (HHC) near the South Tibetan Detachment System in the Sikkim-Darjeeling section has been determined on the basis of thermo-barometric analyses, retrograde breakdown reactions and compositional zoning of garnet. The peak metamorphic condition is estimated to be ~ 10.4 kbar, 800°C from thermo-barometric and phase equilibrium constraints. The observed retrograde breakdown of garnet to spinel and cordierite requires near isothermal and, hence, extremely rapid (~ 15 mm/yr) exhumation up to the depth of ~ 15 km. Numerical modeling suggests that the initial rapid exhumation must have been followed by a much slower process, ~ 2 mm/yr, up to at least ~ 5 km depth, to lead to the development of the observed compositional zoning of garnet. The dramatic change of the exhumation velocity (V_z) might reflect a process of tectonic thinning followed by erosion and/or horizontal flow at shallow depth. Assuming that the V_z did not change significantly below 5 km depth, these results suggest that the HHC samples studied in this work exhumed from a depth of ~ 34 km within ~ 8 Ma. © 2000 Elsevier Science B.V. All rights reserved.

Keywords: Himalayas; Sikkim India; exhumation; crystal zoning; P–T conditions

1. Introduction

The origin and evolution of the Himalayan metamorphic rocks have largely been considered within the framework of the collision of the In-

dian and Eurasian plates during the Eocene (~ 50 Ma), resulting in the subduction of the Indian plate below Tibet and the consequent crustal shortening and deformation, which were accommodated by crustal stacking along a system of intracontinental thrusts and internal deformation of the Indian plate. The thermal evolution and exhumation of these metamorphic rocks have been subjects of extraordinary interests among a large group Earth Scientists as these record the thermo-tectonic evolution of rocks in a major collisional and continental subduction environment,

* Corresponding author. Tel.: +1-520-621-6006;
Fax: +1-520-621-2672; E-mail: ganguly@geo.arizona.edu

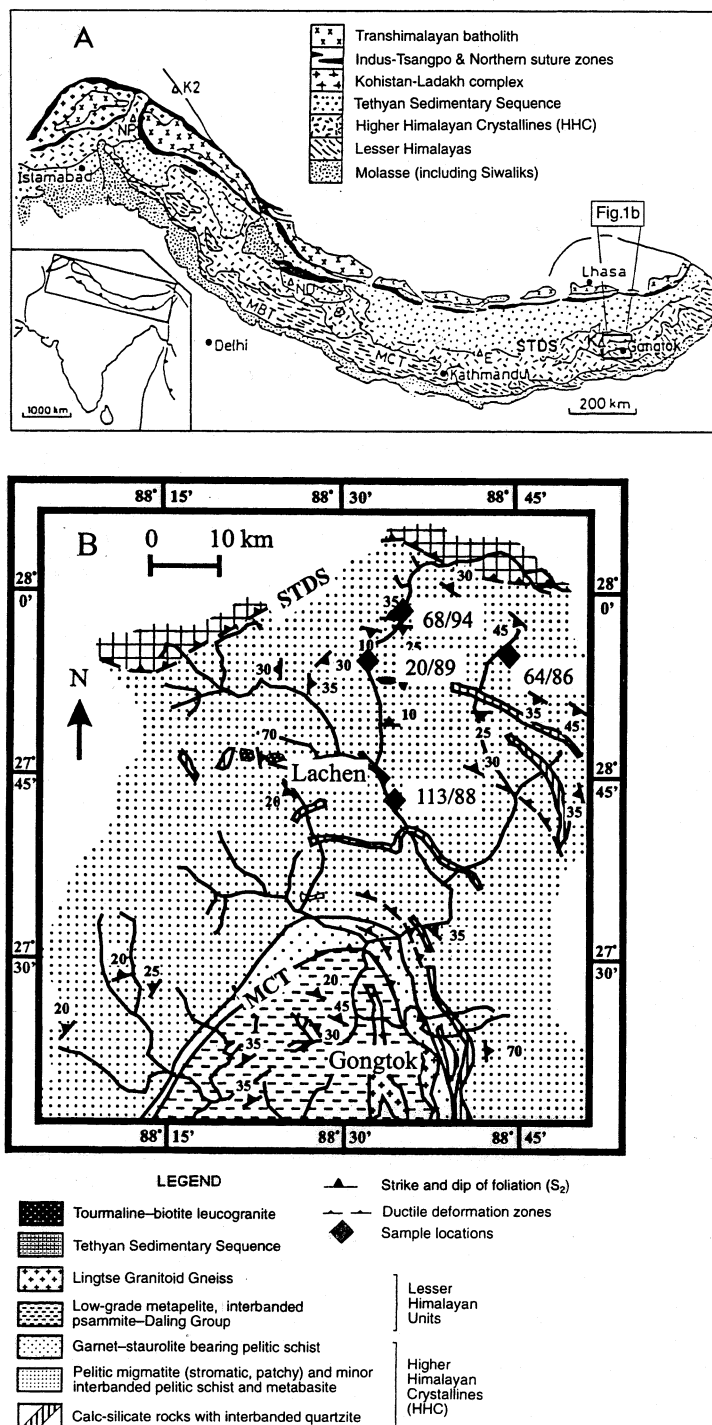


Fig. 1. (A) Generalized map of the Himalayas showing different geotectonic domains and the lithounits. MBT: Main Boundary Fault; NP: Nanga Parbat; ND: Nanda Devi; MCT: Main Central Thrust Zone; STDS: South Tibetan Detachment System. (B) Sample locations (filled diamonds) from the Sikkim section used in this work, along with the sample numbers. Modified from Neogi et al. [6].

and also because of the presence of an inverted (Barrovian) metamorphic sequence for ~ 2000 km along the Himalayan belt [1]. Several workers have estimated the exhumation rates of the Himalayan metamorphic rocks in different sections of the belt using absolute age data and the assumed or estimated closure temperatures of the geochronological systems (e.g. [2–4]). However, no attempt has yet been made to retrieve the cooling and exhumation rates from the retrograde compositional zoning in garnets in the high grade metamorphic rocks. High grade garnets often show a homogeneous core and compositional zoning at the rim due to homogenization at the peak metamorphic condition and cation exchange with the surrounding matrix minerals, coupled with relatively slow intragranular diffusion, as the rock cooled during exhumation [5].

In this work, we have constrained the cooling and exhumation history of rock samples from the upper part of the High Himalayan Crystalline Complex (HHC) in the classic Sikkim–Darjeeling section on the basis of the retrograde compositional zoning of the garnet crystals along with phase equilibrium constraints. The HHC is bounded on the south and north by the Main Central Thrust (MCT) zone and the South Tibetan Detachment System (STDS), respectively (Fig. 1). The MCT is a southerly directed (north dipping) thrust (20–23 Ma) whereas the STDS is a northerly directed system of normal faults (16–23 Ma). In the Sikkim region, the lithological units are disposed in an arcuate regional fold pattern. The MCT zone separates the HHC from the Lesser Himalayan low grade metapelites whereas the STDS separates the HHC from the Tethyan sedimentary sequence.

The locations of four samples, Nos. 64/86, 68/94, 20/89 and 113/88, that were used in the present study, are shown in Fig. 1. The first two samples belong essentially to the same structural height in the upper part of the HHC slab, near the contact of HHC with the Tethyan sediments. Petrographically, these are pelitic migmatites, and consist of biotite (defining the foliation), plagioclase, K-feldspar, sillimanite, garnet and quartz as the major minerals. In 68/94, garnets are occasionally surrounded by spinel, quartz and plagioclase

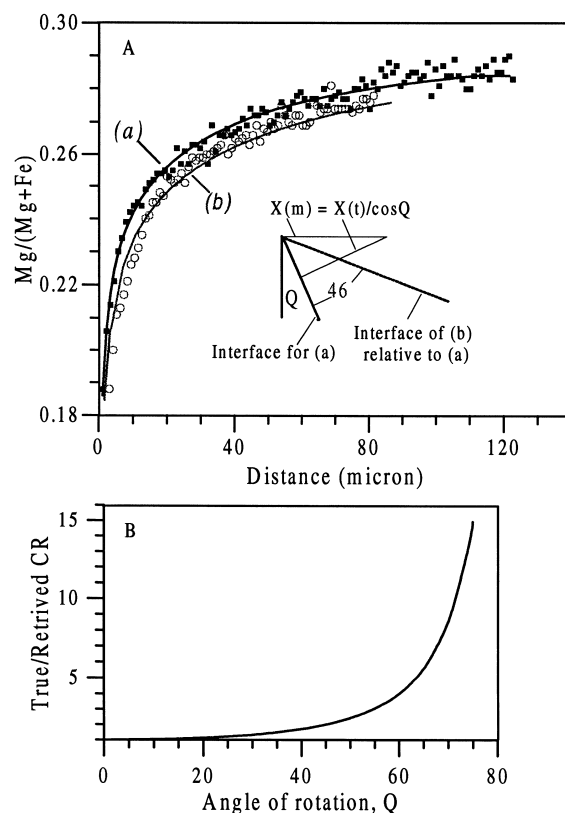


Fig. 2. (A) $\text{Mg}/(\text{Mg}+\text{Fe})$ ratio in garnet as a function of distance from the interface with biotite. The filled squares and open symbols represent compositions measured in two different garnet crystals in the same thin section (sample No. 64/86). The curve (a) is a fit to the filled squares according to the numerical solution of the diffusion equation, as discussed in the text. The curve (b) is derived from (a) by 46° counter-clockwise rotation of the interface, as explained in the inset. $X(m)$ is the measured length of concentration profile when the orientation of the interface deviates from the vertical by an angle Q , and the length of the diffusion profile normal to the interface is $X(t)$. (B) The ratio of the true cooling rate (CR) to that derived from retrograde zoning profile as a function of the angle of rotation of the interface from the vertical.

class symplectites, suggesting the retrograde garnet+sillimanite \rightarrow spinel+quartz [6]. This reaction was also noted in another sample, No. 20/89, which is ~ 10 km south of 68/94. In these rocks the melt was largely segregated from the mineral phases in thin layer parallel bands, and no evidence of retrograde reaction between mineral

phases and melt was found in the specific samples selected for study. The resorption of garnet by reaction with melt ($\text{Gt} + \text{melt} \rightarrow \text{Bt} + \text{Sill} + \text{Qtz}$) was, however, noticed in a sample near Lachen, which is very close to the location of the sample 113/88 ([6], see Fig. 7).

2. Compositional zoning in garnet

2.1. Measurement and selection of zoning profile in garnet

We determined the compositions of a number of garnet crystals in the samples 64/86 and 68/94 by step scanning in an electron microprobe across

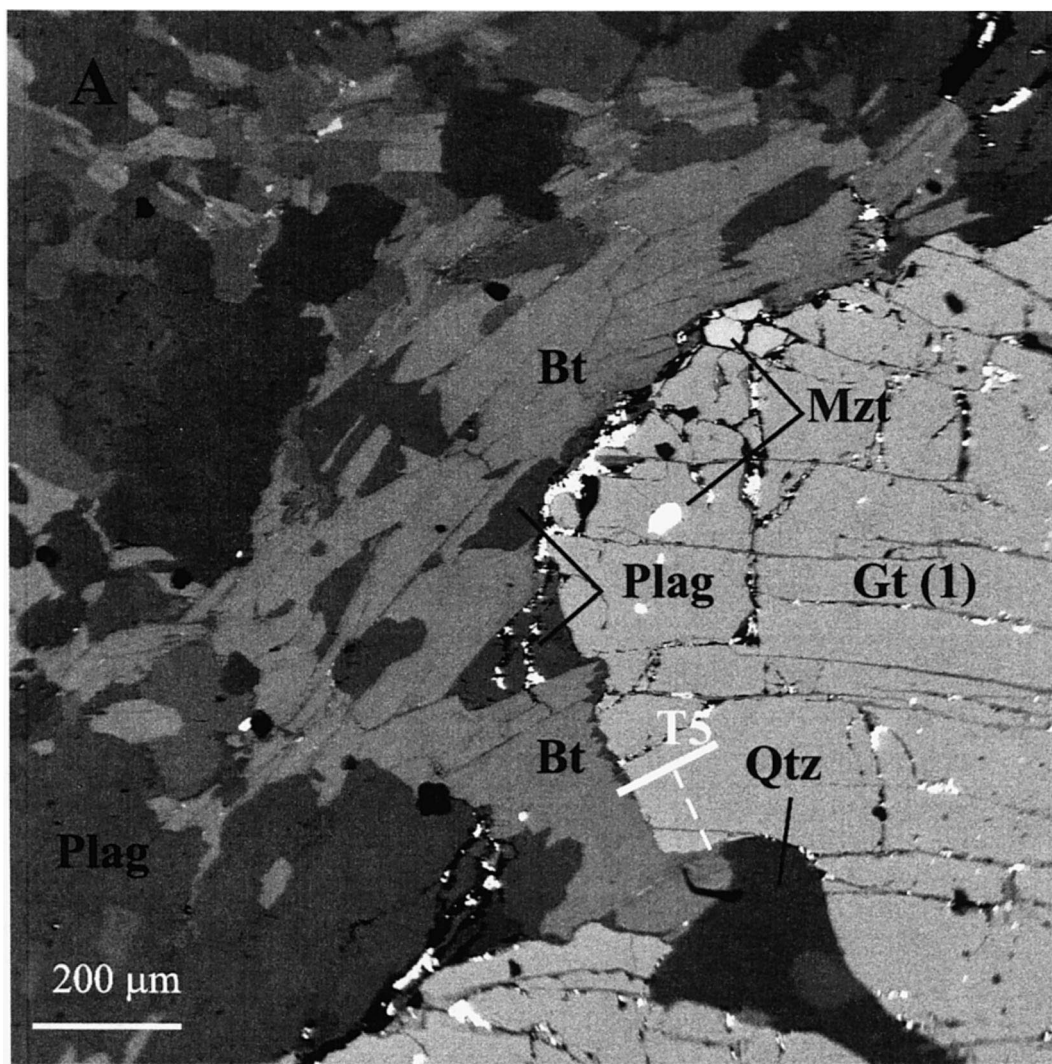


Fig. 3. Backscattered electron images of portions of thin sections illustrating textures and traverses (solid white lines) for the determination of mineral compositions and zoning profiles. Gt: Garnet, Bt: Biotite; Plag: Plagioclase; Qtz: Quartz; Mzt: Monazite; Apt: Apatite; K-Spar: K-feldspar. (A): Garnet in a matrix of biotite, plagioclase and quartz. T5: line traverse along which the zoning profile (a) in garnet, illustrated in Fig. 2a, was measured; zoning was also measured along the dashed line, and was found to be limited to the outer 50 μm of the garnet grain because of the presence of a fracture inside the grain. (B) Mineral association and traverses for composition measurements for the GASP barometry (sillimanite is absent from the field of view).

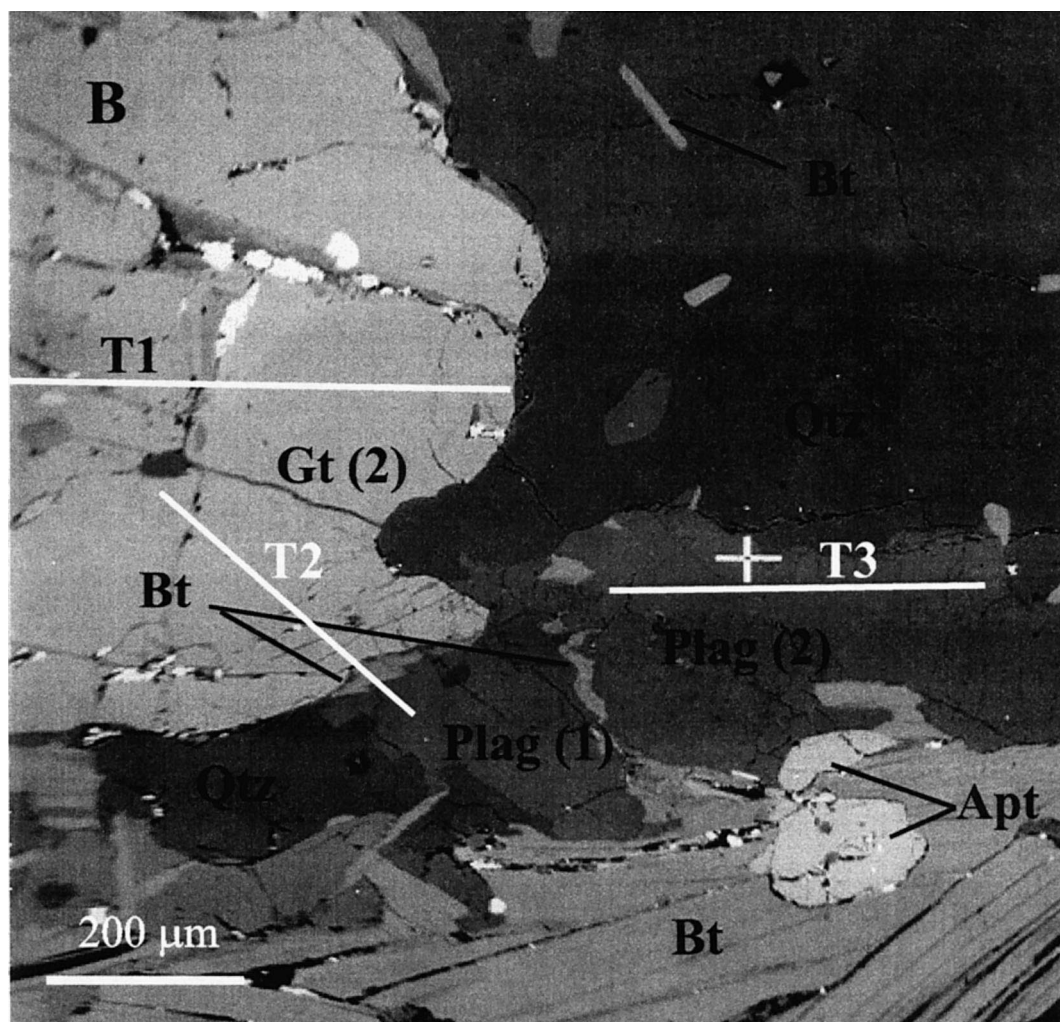


Fig. 3 (continued).

their interface with biotite. The data for the sample 64/86, which were found to be best suited for modeling, are illustrated in Fig. 2A. Fig. 3A shows a backscattered image of the garnet and surrounding matrix and the traverse across the garnet/biotite interface along which the zoning profile (a) in Fig. 2A was measured. The compositional zoning was also measured along the dotted line in Fig. 3A, but was found to be confined to the outer 50 μm probably because of the presence of a fracture in the garnet. The compositions of biotite grains in contact with garnet were homogeneous and were essentially the same as those of

other biotite grains within the same thin section. In modeling the retrograde zoning in garnet, we assumed that the biotite was essentially a homogeneous infinite reservoir of the exchanging components, Fe^{2+} and Mg. In addition to compositional homogeneity, this assumption implies that the mass of biotite was much larger than that of garnet *affected* by cation exchange. Visual inspection of the thin sections suggests that this requirement was easily satisfied (Fig. 3A).

Ideally, the compositional zoning in a crystal used for retrieving the cooling rate should be measured along a direction which is normal to the

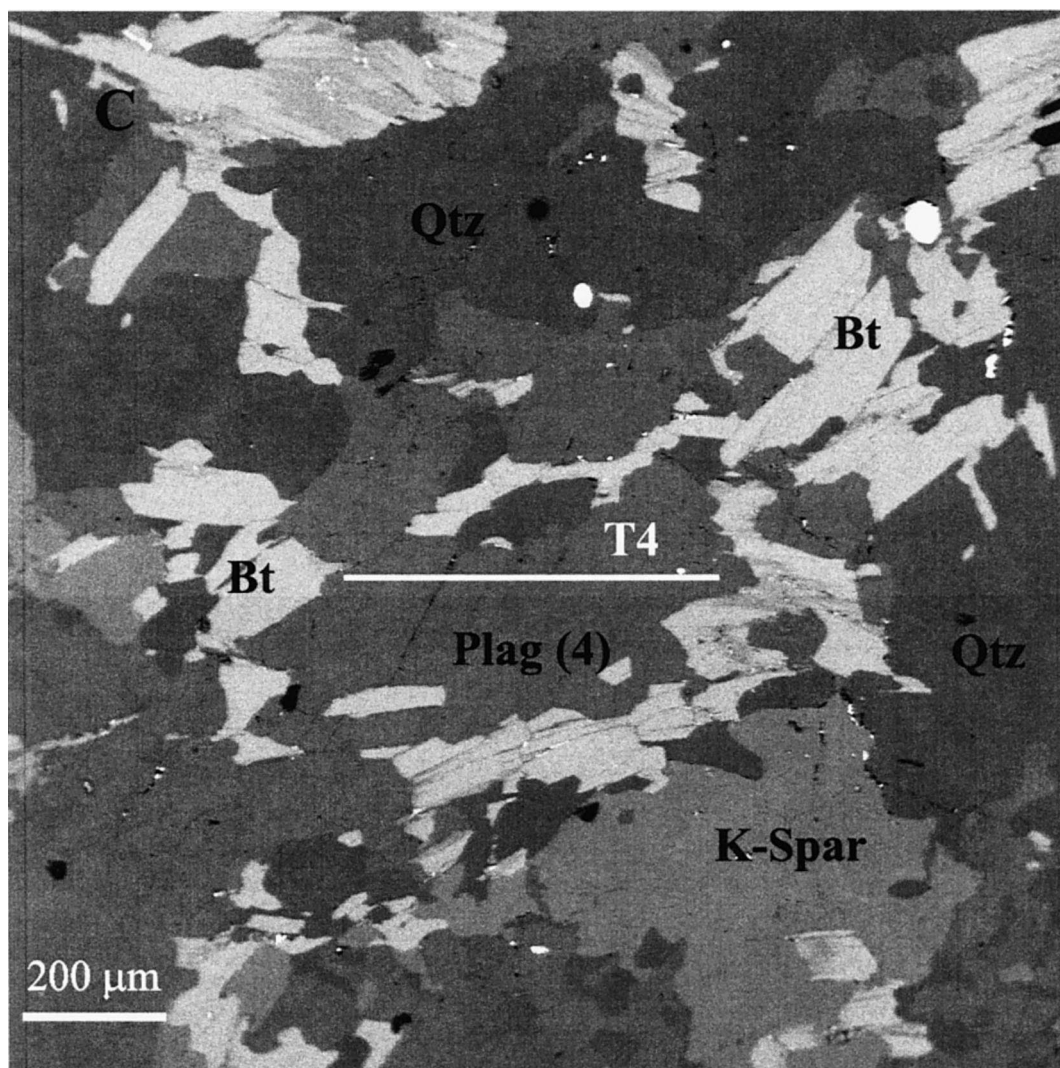


Fig. 3 (continued).

interface. However, in a thin section one can only assure the normalcy of the direction with respect to the trace of the interface. If the chosen traverse were not normal to the interfacial *plane*, then the length of the measured concentration profile would be longer than that due to diffusion normal to the plane and, consequently, the retrieved cooling rate would be slower than the true cooling rate. The most definitive way to ensure normalcy of the traverse with respect to the interfacial plane is to obtain a three-dimensional image of the rock

by computer aided X-ray tomography, and cut the thin section normal to the interfacial plane [7]. In this work, however, we have taken a simpler approach, which is as follows.

We measured a number of concentration profiles in garnet in contact with biotite in the samples 64/86 and 68/94, and chose the shortest profile for modeling the cooling rate from the appropriate solution of the diffusion equation. (The profiles were measured by step scanning in an electron microprobe using the following stan-

dards: synthetic pyrope, grossular, spessartine and diopside for Mg, Ca, Mn and Si, respectively; natural olivine, jadeite, sphene, chromite, feldspar for Fe, Na, Ti, Cr, K, respectively, and Ni-diopside glass for Ni.) The shortest concentration profile was found in the sample 64/86. This and another longer profile from the same thin section is shown in Fig. 2A. The curves (a) and (b) fit the data in the shorter (filled squares) and longer (circles) profiles, respectively. However, the curve (b) was generated from (a) by a 46° counterclockwise rotation of the interface (as illustrated in the inset of Fig. 2A). Thus, we conclude that the interface of the garnet crystal which yielded the concentration profile fitted by the curve (b) was rotated counterclockwise by an angle of $\sim 46^\circ$ from that of the other garnet crystal. These two crystals will henceforth be referred to as crystals B and A, respectively. We also analyzed the effect of distortion of the concentration profile, due to rotation of the interface from the vertical, on the calculation of cooling rate. The results, which are illustrated in Fig. 2B, show that the effect is negligible up to $\sim 30^\circ$ rotation of the interface, especially considering the various uncertainties that enter into the cooling rate calculation. Thus, if we make the reasonable assumption that the interface of the crystal B was not rotated by more than 75° from the vertical, then it follows that the interface of the crystal A was within 30° from the vertical. Thus, the cooling rate retrieved from curve (a) should represent a very close lower bound to the true cooling rate.

2.2. Modeling of the retrograde compositional zoning

Lasaga [5] developed a theory to retrieve the cooling rate from retrograde compositional zoning in a mineral with a planar interface with an adjacent phase. In what follows, we used the general framework of his approach, with some modifications, which are appropriate to the present problem, along with implementation of a numerical code and an optimization code, as discussed below. The modifications concern incorporation of a nonlinear cooling model, which permits a

more straightforward derivation of the governing equations than through the use of a linear cooling model [5] and the development of the equation governing the variation of interface composition as a function of time during cooling. The composition of garnet at the boundary adjacent to biotite was assumed to be in equilibrium with biotite during the cooling process, and, in addition, biotite composition was assumed to have remained fixed, as suggested by the observational data.

Since Fe^{2+} and Mg are the only species which exchange significantly between garnet and biotite, the development of retrograde compositional zoning in garnet adjacent to biotite can be treated as a binary diffusion problem with time dependent interdiffusion coefficient, $D(t)$. For simplicity, we assumed that the interdiffusion coefficient, $D(\text{Fe-Mg})$, is independent of composition within the range of the observed compositional variation in garnet from the core to the rim (Fig. 2). The time dependence of D can be expressed as $D(t) = D(T_0)f(t)$, where $D(T_0)$ is the interdiffusion coefficient at the initial temperature, T_0 . By defining a new time variable, t' , as:

$$dt' = f(t)dt \quad (1)$$

and dimensionless time and distance variables as, respectively:

$$t'_r = \frac{D(T_0)t'}{a^2}, \text{ and } x'_r = \frac{x}{a} \quad (2)$$

where x is the distance normal to the planar interface and a is a specific distance within the medium where $dC/dx = 0$ (i.e. $dC/dx_r = 0$ at $x_r = 1$), the one dimensional diffusion equation reduces to:

$$\frac{dC}{dt'_r} = \frac{d^2C}{dx'^2_r} \quad (3)$$

It can be shown [5] that, in general:

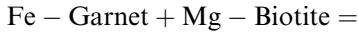
$$D(t) = D(T_0)\exp\left[-\frac{Q}{R}\left(\frac{1}{T}-\frac{1}{T_0}\right)\right] = D(T_0)f(t) \quad (4.1)$$

and

$$K(t) = K(T_0) \exp \left[-\frac{\Delta H^0}{R} \left(\frac{1}{T} - \frac{1}{T_0} \right) \right] \quad (4.2)$$

where Q is the activation energy of diffusion, K and ΔH^0 are the equilibrium constant and enthalpy change of a reaction, respectively, and $K(T_0)$ is the equilibrium constant at T_0 .

The equilibrium fractionation of Fe and Mg between garnet and biotite is governed by the exchange reaction:



where Fe-garnet is the ferrous iron end member of garnet written on the basis of 1 mol of Fe^{2+} per formula unit, and similarly for the other components. The equilibrium constant for this reaction is:

$$K = \left[\frac{(\text{Mg/Fe})^{\text{Gt}}}{(\text{Mg/Fe})^{\text{Bt}}} \right] \left[\frac{(\lambda_{\text{Mg}}/\lambda_{\text{Fe}})^{\text{Gt}}}{(\lambda_{\text{Mg}}/\lambda_{\text{Fe}})^{\text{Bt}}} \right] \quad (5)$$

where λ_i^α is the activity coefficient of the divalent cation i in the phase α . However, since Fe^{2+} -Mg mixing in both biotite and garnet are close to ideal [8,9], the term within the second square bracket is set to unity.

Assuming that the reciprocal temperature changes linearly with time, i.e.

$$\frac{1}{T} = \frac{1}{T_0} + \eta t \quad (6)$$

where η is a cooling time constant (with the dimension of $\text{K}^{-1} \text{t}^{-1}$), we have, from Eq. 4.2:

$$K(T) = K(T_0) e^{-\beta t} \quad (7)$$

where

$$\beta = \frac{\Delta H^0 \eta}{R} \quad (8)$$

Combining Eqs. 5 and 7, and imposing the condition that the composition of biotite had remained fixed, we now obtain:

$$X_{\text{Mg}}^{\text{Gt}}(t) = X_{\text{Mg}}^{\text{Gt}}(T_0) \left[\frac{(1 - X_{\text{Mg}}^{\text{Gt}}(t))}{(1 - X_{\text{Mg}}^{\text{Gt}}(T_0))} \right] e^{-\beta t} \quad (9)$$

where $X_{\text{Mg}} = \text{Mg}/(\text{Mg} + \text{Fe}^{2+})$.

Expressing $f(t)$ according to Eqs. 4.1 and 6, and substituting in Eq. 1, we have:

$$dt' = \exp \left[-\frac{Q\eta t}{R} \right] dt \quad (10)$$

so that

$$t' = \frac{1}{\gamma} (1 - e^{-\gamma t}) \quad (11)$$

where

$$\gamma = \frac{Q\eta}{R} \quad (12)$$

From Eqs. 2, 9 and 11, one can derive:

$$X_{\text{Mg}}^{\text{Gt}}(t) = X_{\text{Mg}}^{\text{Gt}}(T_0) \left[\frac{(1 - X_{\text{Mg}}^{\text{Gt}}(t))}{(1 - X_{\text{Mg}}^{\text{Gt}}(T_0))} \right] (1 - \gamma' t')^{\beta/\gamma} \quad (13)$$

where

$$\gamma' = \frac{a^2 \gamma}{D(T_0)} = \frac{a^2 Q \eta}{RD(T_0)} \quad (14)$$

Referring to Eqs. 8 and 12, it is easy to see that the quantity $\beta/\gamma = \Delta H^0/Q$.

Lasaga [5] gave an analytical solution of Eq. 3 subject to the conditions that (a) the change of interface composition is given by Eq. 13, but setting the term within the square brackets to unity, (b) $dC/dx_r = 0$ at $x_r = 1$, and (c) the phase had a homogeneous composition at the initial temperature T_0 . However, this solution converges quite slowly [10]. A rapid convergence was needed for our modeling approach as it involved the calculation of numerous profiles using a permissible range of values of β/γ and the initial composition to find the optimal solution that best fit the data on retrograde zoning profile. We, thus, solved Eq. 3 using the Crank–Nicolson implicit finite difference scheme [11], which leads to an even more

rapid convergence than the explicit finite difference scheme used in [10]. The interface composition of garnet was evaluated numerically at every time step from Eq. 13. The results of the modeling of the zoning profile differed significantly from the case when this term is set equal to unity [5].

From the experimentally determined data on the ΔH^0 of the equilibrium (a) [12] and the self-diffusion coefficients, D^* , of Fe and Mg in garnet [13], we obtain β/γ (i.e. $\Delta H^0/Q$) = 0.03 ± 0.02 at 4 kbar, where the uncertainty represents one standard deviation, σ . (The pressure of 4 kbar was chosen in accordance with the model of development of compositional zoning, as discussed later.) The activation energy for the Fe²⁺-Mg interdiffusion was obtained by first calculating, according to Manning [14], $D(\text{Fe-Mg})$ at several temperatures from the self diffusion coefficients, $D^*(\text{Fe})$ and $D^*(\text{Mg})$, at the composition of $X_{\text{Mg}} = 0.23$ (\sim half-way between the core and rim compositions) and regressing the $\ln D(\text{Fe-Mg})$ values against $1/T$. This yields, at $X_{\text{Mg}} = 0.23$, $D(\text{Fe-Mg}) = 4.33 \times 10^{-5} \text{e}^{-Q(P)/RT}$ cm²/s, where $Q(P) = 65090 + 132 \times P$ (kbar).

The finite difference scheme for the solution of Eq. 3 and the permissible range of the values for β/γ within $\pm 2\sigma$ range was interfaced with an optimization program, MINUIT [15]. The initial composition, $X(T_0)$, was also allowed to vary to a specified level above the measured core composition of garnet (i.e. the calculations were not subject to the condition that the measured core composition of garnet reflects its initial composition at T_0). From a calculation of numerous profiles within the above constraints, the optimization program found the optimal combination of β/γ and $X(T_0)$ which led to the best match between the calculated and measured concentration profiles by minimizing the sum of the squares of the differences between the two. This exercise yielded $\beta/\gamma = 0.048$ and $\gamma' = 1.84$ for $a = 128$ μm . The calculated profile according to these parameters is compared with the measured zoning data in Fig. 2A (curve (a) and the filled squares). Even though the program was free to choose the initial composition of garnet, the optimization program did not return an initial composition that was significantly different from the measured core

composition of the garnet. This suggests that the core composition of the garnet crystal was not significantly affected during cooling. We shall return to this point later.

Using Eq. 14, one can calculate the cooling time constant, η , for an asymptotic cooling model from the above value of γ' and a knowledge of the peak metamorphic temperature, T_0 (assuming that the change of pressure during cooling did not have any significant effect on D). However, we note that for large time:

$$\gamma' = \frac{a^2}{\int_0^t D(\tau) d\tau} \quad (15)$$

[16], and that the value of the above integral is independent of the T - t path. Thus, one can quantify the cooling path according to any prescribed model such that the value of this integral calculated by applying the diffusion data to this path equals its value recovered from γ' . This approach was followed to calculate the cooling and exhumation rates, as discussed below. Lindström et al. [10] noted that the value of γ' depends on the value of a that is used in the calculation, but the same cooling rate is obtained from each combination of γ' and a . The reason for this invariance of the calculated cooling rate is obvious from the above discussion since the cooling rate is obtained from the ratio of γ' to a^2 (Eq. 14), which is invariant (Eq. 15).

3. Phase equilibria

3.1. Peak metamorphic condition

Using the observed mineral assemblage, the peak P - T condition can be constrained by the simultaneous solution of the conditions of equilibrium of the exchange reaction (a) and of the equilibrium $\text{Gt} + 2\text{Sill} + \text{Qtz} = 3\text{Plag}$, which is commonly referred to by the acronym GASP. Fig. 3 shows the backscattered electron images of different areas of the thin section which were analyzed by electron microprobe to select compositions for the purpose of thermo-barometric calculations.

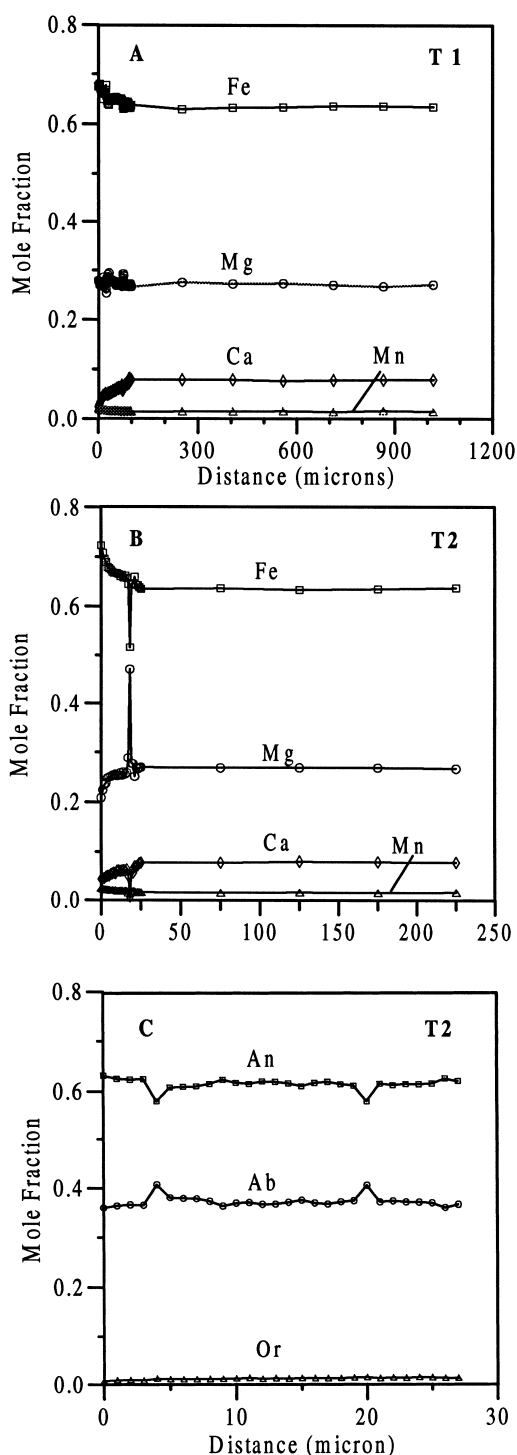


Fig. 4. Compositional profiles of garnet along the traverses (A) T1, (B) T2 and of (C) plagioclase along T2 in Fig. 3b.

Compositional zoning was measured along the indicated line traverses (T1–T5) within the garnet and plagioclase grains. The compositional data for garnet along the traverse T1 and those for garnet and plagioclase along T2 (Fig. 3B) are illustrated in Fig. 4. Along T2, the garnet shows a weak zoning near the rim, but is otherwise homogeneous, whereas the plagioclase is essentially homogeneous in composition. The zoning in garnet is even weaker along the traverse T1. This difference in the extent of zoning is due to the nature of the adjacent matrix phase (that is a very small grain of biotite in the traverse T2 and quartz at the end of T1). There is no significant difference between the core compositions of the garnet grains shown in Fig. 3A,B. Plagioclase composition along the traverses T3 and T4 (Fig. 3B,C) is homogeneous and is essentially the same as that along T2 (Fig. 3A).

The compositional and textural data discussed above suggest that the growth zoning of Fe, Mg, Ca and Mn in the garnet grains, which are ~ 500 μm or less in radial dimension, were completely homogenized at or near the peak P – T condition and that the garnets subsequently developed compositional zoning by exchange with the matrix phases, primarily biotite, either through direct exchange across the interface or through grain boundary diffusion when biotite was not in direct contact. (The compositional data of garnet along T1 and T2 imply that the rates of grain boundary diffusion of the divalent cations were not effectively instantaneous compared to those of volume diffusion in garnet. On the other hand, the rates of volume diffusion in biotite must have been very rapid compared to those of grain boundary diffusion leading to the observed homogeneity of the biotite composition.) Garnets also have plagioclase *inclusions* which provide unequivocal evidence that plagioclase was present during garnet growth. The close similarity of composition between plagioclase grains very close to garnet and away from it suggests that the analyzed plagioclase grains were not produced by the breakdown of garnet after it had developed compositional zoning. We have, thus, used the core composition of garnet along with the compositions of the adjacent biotite, where it was present in large abun-

dance to ensure retention of the peak composition (Fig. 3A), and of plagioclase (Fig. 3B) grains to calculate the peak metamorphic P – T condition. These data are presented in Tables 1 and 2.

The garnet and plagioclase solution properties were treated according to [9,17], respectively. For the garnet–biotite thermometry, we used the recent formulations [9] and [18]. We did not analyze for the Fe^{3+} in garnet and biotite, but assumed that 3 mol% of total iron in garnet and 11.6 mol% of that in biotite were in the Fe^{3+} state, in accordance with the average values for the regionally metamorphosed metapelites [18]. As illustrated in Fig. 5, the solution for the equilibrium coexistence of sillimanite, plagioclase, biotite and quartz with garnet having an initial composition given by its measured core composition yields ~ 10.4 kbar, 800°C as the peak metamorphic condition. Equat-

ing $\text{Fe}(\text{total})$ to Fe^{2+} yields $\sim 50^\circ\text{C}$ higher temperature.

3.2. Retrograde reactions

An additional constraint on the exhumation path is provided by the retrograde reactions of garnet, which can be deciphered from detailed petrographic studies. Two samples, 68/94 and 20/89, show retrograde breakdown of garnet to spinel. Since these samples are from the same metamorphic zone as 64/86 (Fig. 1), which contains the garnet crystals subjected to the modeling of retrograde compositional zoning, and there is no field evidence whatsoever of any structural break between these samples, it is reasonable to assume that all three samples were subjected to the same exhumation history. We, thus, develop

Table 1
Selected compositions of garnet and biotite in the sample 64/86

Wt%	Garnet (1)		Biotite			
	rim	core	adjacent to Gt (1)	domain 1	domain 2	domain 3
FeO	33.90	30.41	16.76	16.88	17.05	17.50
MgO	4.42	6.85	11.34	11.35	11.32	11.25
MnO	1.94	0.83	0.15	0.02	0.06	0.08
CaO	1.67	2.78	0.07	0.00	0.00	0.07
Cr_2O_3	0.01	0.01	0.04	0.07	0.07	0.08
NiO	0.02	0.01	0.02	0.04	0.12	0.03
TiO_2	0.05	0.01	3.42	4.39	4.44	4.23
Na_2O	0.03	0.01	0.17	0.17	0.19	0.18
K_2O	0.03	0.00	8.86	9.64	9.76	9.80
Al_2O_3	21.01	21.62	18.30	17.51	17.73	17.84
SiO_2	37.18	38.31	36.66	36.29	36.66	36.64
Total cations	100.27	100.84	95.79	96.35	97.39	97.67
Fe	2.26	1.97	1.02	1.03	1.03	1.05
$\text{Fe}^{2+\text{a}}$	2.19	1.91	0.90	0.91	0.91	0.93
Mg	0.52	0.79	1.23	1.23	1.22	1.21
Mn	0.13	0.05	0.01	0.00	0.00	0.01
Ca	0.14	0.23	0.01	0.00	0.00	0.00
Cr	0.00	0.00	0.00	0.00	0.00	0.00
Ni	0.00	0.00	0.00	0.00	0.01	0.00
Ti	0.00	0.00	0.19	0.24	0.24	0.23
Na	0.00	0.00	0.03	0.02	0.03	0.03
K	0.00	0.00	0.82	0.90	0.90	0.90
Al	1.97	1.98	1.57	1.50	1.51	1.51
Si	2.96	2.97	2.67	2.64	2.64	2.64

The cation proportions in garnet and biotite are on 12 and 11 oxygen basis, respectively. Garnet (1) and adjacent biotite are shown in Fig. 3a. Other biotite compositions are in three different domains of the same thin section.

^aGarnet: $\text{Fe}^{2+} = 97\%$ of total Fe. Biotite: $\text{Fe}^{2+} = 88.4\%$ of total Fe.

Table 2

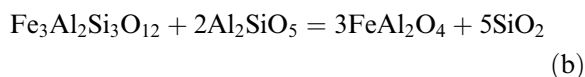
Compositions of garnet and plagioclase in the sample 64/86

Wt%	Garnet (2)	Plagioclase			
	core	1	2	3	4
FeO	29.96	0.16	0.03	0.03	0.04
MgO	7.07	0.02	0.00	0.00	0.00
MnO	0.75	0.01	0.01	0.01	0.01
CaO	2.82	7.69	7.37	7.42	7.38
Na ₂ O	0.01	7.04	7.37	7.34	7.41
K ₂ O	0.00	0.22	0.37	0.35	0.33
Al ₂ O ₃	22.31	27.04	26.52	26.54	26.54
SiO ₂	38.07	57.93	57.99	57.91	58.62
Total cations	100.99	100.12	99.65	99.59	100.32
Fe	1.93	0.01	0.00	0.00	0.00
Mg	0.81	0.00	0.00	0.00	0.00
Mn	0.05	0.00	0.00	0.00	0.00
Ca	0.23	0.37	0.35	0.36	0.35
Na	0.00	0.61	0.65	0.64	0.64
K	0.00	0.01	0.02	0.02	0.02
Al	2.21	1.42	1.40	1.40	1.39
Si	2.94	2.58	2.59	2.59	2.60

Garnet (2) and plagioclase (1) and (2) are shown in Fig. 3b; plagioclase (3) is adjacent to plagioclase (2), but outside the field of view; plagioclase (4) is shown in Fig. 3c. The cation proportions in garnet and plagioclase are on 12 and 8 oxygen basis, respectively.

an integrated exhumation history for these samples by combining the constraints imposed by the compositional zoning and breakdown reaction of garnet during exhumation.

The retrograde reaction of garnet to spinel is given by:



in which sillimanite and quartz are essentially pure phases. Thus, using an ionic solution model [9] and a standard state of pure component at the P and T of interest for each phase, the equilibrium constant for this reaction is expressed as:

$$K_b = \left(\frac{X_{\text{Fe}}^{\text{sp}}}{X_{\text{Fe}}^{\text{Gt}}} \right)^3 \left(\frac{\lambda_{\text{Fe}}^{\text{sp}}}{\lambda_{\text{Fe}}^{\text{Gt}}} \right)^3 \quad (16)$$

where X and λ stand, respectively, for the atomic fraction and the activity coefficient of the specified component on 1-cation basis. The breakdown reaction texture of garnet to spinel in 20/89 was

described by Neogi et al. ([6], Fig. 12), who also gave the compositions of the garnet rim and coexisting spinel. Using these compositions, the ratio of the atomic fraction of Fe^{2+} in spinel to that in garnet is found to be essentially ~ 1 . Using the garnet mixing model in [9], we get $\lambda_{\text{Fe}}^{\text{Gt}} \sim 1.02$ at 800°C , 4 kbar for the given garnet composition of $\text{Alm}_{66}\text{Py}_{27}\text{Gr}_3\text{Spess}_3$. The spinel has the composition of $\sim (\text{Fe}_{0.66}\text{Mg}_{0.24}\text{Zn}_{0.10})\text{Al}_2\text{O}_4$. From experimentally determined Fe^{2+} –Mg partitioning between spinel and olivine, O'Neill (personal communication) derived a regular solution Fe–Mg interaction parameter (W_{FeMg}) ~ 2.5 kJ/mol for spinel. This small deviation from ideality is consistent with our recent study of Fe–Mg distribution between spinel and orthopyroxene as a function of temperature and composition [19] and the mixing property of orthopyroxene [20]. There are, however, no data on the mixing property of the Zn component in spinel. Nonetheless, the effect of ~ 10 mol% Zn component on λ_{Fe} in spinel can be approximately evaluated as follows.

Assuming a regular solution type behavior [8]

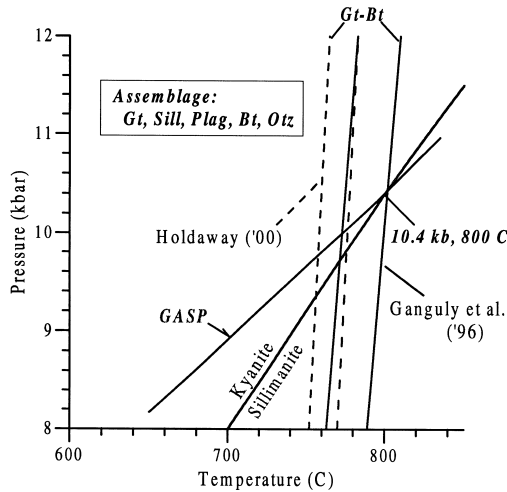


Fig. 5. Determination of the peak P – T condition of the sample 64/86 on the basis of the thermo-barometric analysis of the assemblage garnet, biotite, sillimanite, plagioclase and quartz. Gt–Bt: P – T relations defined by the compositional properties of garnet-core and biotite, according to the recent formulations of Ganguly et al. [9] and Holdaway [18], which are indicated by solid and dashed lines, respectively. GASP: equilibrium boundary for the reaction $\text{Grt} + 2\text{Sill} + \text{Qtz} = 3\text{Plag}$.

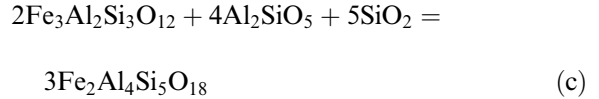
for the ternary spinel, we have

$$RT \ln \lambda_{\text{Fe}} = W_{\text{FeMg}}(X_{\text{Mg}})^2 + X_{\text{Mg}}X_{\text{Zn}}(W_{\text{FeZn}} + W_{\text{FeMg}} - W_{\text{MgZn}}) \quad (17)$$

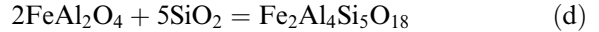
Now in tetrahedral coordination, the ionic radii of Fe and Zn are quite similar, 0.63 and 0.60 Å, respectively, whereas that of Mg is 0.49 Å. It is, therefore, reasonable to expect that in spinel $W_{\text{FeMg}} \approx W_{\text{ZnMg}}$ and $W_{\text{FeZn}} \approx 0$, so that the sum of the W terms within the second parentheses of Eq. 17 should be quite small. Furthermore, since $X_{\text{Mg}}X_{\text{Zn}} \sim 0.02$, the last term in Eq. 17 should be expected to have quite a small effect on λ_{Fe} in spinel. Using the above value for W_{FeMg} in spinel, we then have $\lambda_{\text{Fe}}(\text{spinel}) \sim 1.02$ at 800°C. Consequently, $K_b \sim 1$, which implies that the P – T location of the equilibrium (b) for the composition of the sample 20/89 is not significantly different from that in the end member system (FAS) $\text{FeO} - \text{Al}_2\text{O}_3 - \text{SiO}_2$ [21].

At lower temperature, the low pressure limit of garnet stability in the same system is defined by

the breakdown reaction to cordierite:



The intersection of the equilibria (b) and (c) leads to another univariant equilibrium:



The P – T configurations of these equilibria in the FAS system [21] are shown in Fig. 6. Only the retrograde reaction (b) was, however, observed in the above samples. Cordierite was found in 20/89, but it was not related to garnet by any clear cut reaction texture. However, it must have formed by the breakdown of garnet since the calculated peak P – T condition of this sample, according to GASP and garnet–biotite exchange equilibrium, is very similar to that of 64/86, which is discussed above. These observations suggest

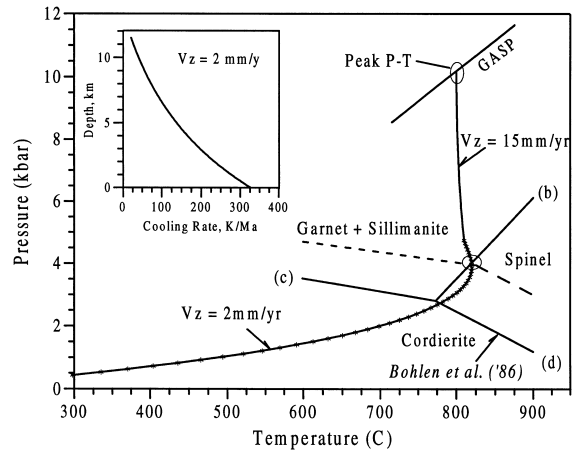


Fig. 6. Two step exhumation paths (solid and patterned lines) and the corresponding velocities of the samples, as reconstructed from the phase equilibrium constraints and retrograde zoning in garnet. The inset shows the cooling rate as function of depth for $V_z = 2$ mm/yr, which was required to produce the retrograde compositional zoning in garnet (Fig. 2a). The solid lines labeled (b), (c) and (d) denote the equilibrium reaction boundaries in the FAS system [20]. The corresponding dashed lines represent the calculated displacements of the equilibria in the natural compositions. The equilibrium (b) is not significantly affected by the change of mineral compositions in the natural assemblage.

that the P – T path during exhumation of the HHC samples exceeded the garnet stability field at a P – T condition which is close to that of the invariant point defined by the intersections of the equilibria (b), (c) and (d) for the natural composition (Fig. 6). Determination of this invariant point requires calculation of one additional equilibrium, (c) or (d), for the natural compositions. For this purpose, we make use of the petrographic observation and composition in another sample, No. 113/88, which is ~ 20 km south of the samples considered above (Fig. 1). In this sample, garnet was found to have partially broken down to cordierite according to the reaction (c) (see Fig. 11 in [6]).

Using the compositional data for the coexisting garnet and cordierite [6], the garnet solution model in [9], and assuming that $W_{\text{FeMg}}(\text{cordierite}) = 1.83$ kJ/mol [22], we calculated (Fig. 6) the displacement of the equilibrium (c) from that in the FAS system [21]. Since the garnet composition in the sample 113/88 is somewhat more Fe rich than that in 20/89 ($X_{\text{Fe}} = 0.76$ and 0.66 , respectively), the stability of garnet with respect to cordierite in 20/89 is likely to lie at a somewhat higher pressure than that calculated for 113/88. For the present purpose, we treat the garnet/cordierite boundary calculated for the sample 113/88 as an approximation to the stability of garnet in 20/89 with respect to cordierite. The displaced spinel/cordierite boundary in Fig. 6 (curve (d)) is drawn subparallel to the boundary in the FAS system through the displaced position of the invariant point.

4. Exhumation history

4.1. Exhumation and cooling rates

Fig. 6 shows a comparison of the estimated peak P – T condition of the sample 64/86 with the condition for breakdown of garnet+sillimanite to spinel, as observed in other samples (68/94 and 20/89) from the same structural height and metamorphic grade. These data suggest a near isothermal and, hence, a very rapid exhumation for approximately the first 20 km. During this period, the compositional property of garnet should have

remained essentially unmodified since the process was extremely rapid, and also there would have been no significant change of Fe–Mg fractionation between garnet and biotite, which drives the development of compositional zoning in garnet. The development of retrograde compositional zoning in garnet requires that the exhumation rate must have slowed down greatly after the retrograde P – T path intersected or came near the garnet/spinel reaction boundary.

Assuming that there is no lateral change of temperature, the P – T path associated with a fixed exhumation velocity and constant thermal diffusivity of the rock can be calculated by solving the one dimensional conduction-convection equation:

$$\frac{\partial T}{\partial t} = k \frac{\partial^2 T}{\partial Z^2} + V_z \frac{\partial T}{\partial Z} + \frac{A(Z)}{\rho C_p} \quad (18)$$

where Z is depth, V_z is the velocity, positive upwards, k is the thermal diffusivity, $A(Z)$ is the heat production rate per unit volume, ρ is the density and C_p is the isobaric specific heat capacity. The quantity ρC_p is assumed to be constant ($\rho = 2750$ kg/m³ and $C_p = 880$ J/kg K). Z was converted to P according to [23]. The solution of Eq. 18 for the special case of a semi-infinite slab with a constant value of A , a fixed temperature at the surface and a linear initial geotherm is given by Carslaw and Jaeger ([24], p. 388), and used by others [25,26] for the calculation of P – T paths during exhumation of rocks. In this solution T is expressed in terms of Z , V_z and t , but the last three variables are also linked by the relation $Z = Z_0 - V_z t$ where Z_0 is the initial depth. England and Thompson [26] showed that the results obtained from the solution in [24] approximate quite well the results of more detailed numerical calculations using nonlinear initial geotherm and a boundary condition of constant heat flux at large depth in the mantle.

We assumed that the radioactive heat production as a function of depth followed the Birch–Lachenbruch relation, i.e. $A(Z) = A_0 e^{-Z/D}$, where D is a scaling depth within which the heat producing elements are primarily concentrated. The $P(Z)$ – T path during exhumation for a given value of the velocity was then calculated using the ana-

lytical solution in [24], but by dividing the total depth into a large number of layers and assuming that A was constant within each layer, and equaled its average value within the layer. England et al. [27] summarized the available data on the radioactive heat production of the exposed HHC rocks in the Annapurna-Manaslu region of central Nepal. These data yield an average value of $A_0 \sim 2.66 \mu\text{W/m}^3$. From the data of Gupta et al. [28] for the Indian shield, D was taken to be 12 km. $T(Z_i)$ was calculated by assuming that the initial temperature profile at Z_{i-1} was linear, matching the temperature calculated from the previous step.

Using now $k = 1 \text{ mm}^2/\text{s}$, a two stage exhumation process was constructed (Fig. 6) so that the P – $T(t)$ path from the peak metamorphic condition not only matches the constraint imposed by the observed retrograde breakdown of garnet but also leads to the observed retrograde zoning profile in garnet (Fig. 2A). The solution of Eq. 18 with $V_z \sim 15 \text{ mm/yr}$ leads to a near isothermal P – T path from the peak condition. A number of P – T paths were calculated by reducing the velocity when the rocks reached a depth of 14.7 km, and $\int D dt$ was evaluated along each path using the Fe–Mg interdiffusion data of garnet. The latter was calculated [13,14] from the self diffusion data of Fe and Mg [13] at the median composition within the diffusion zone, and was assumed to be independent of compositional variation within this zone (Fig. 2A). A value $V_z = 2 \text{ mm/yr}$ was found to lead to a P – $T(t)$ path which yields $\int D dt$ matching that retrieved from the retrograde compositional zoning of garnet (i.e. $8.18 \times 10^{-5} \text{ cm}^2/\text{s}$). The temperature calculated from the rim composition of the zoned garnet (Fig. 2A) and the adjacent biotite composition is $\sim 450^\circ\text{C}$. This is approximately the temperature at which Fe–Mg exchange between garnet and biotite effectively ceased. Thus, the calculated $V_z = 2 \text{ mm/yr}$ does not necessarily apply below 450°C .

In the simulation of the second stage of the exhumation process, there is a small segment in the P – T path in which the rocks heat slightly during exhumation and then cools (Fig. 6) because the heating by the radioactive heat produc-

tion outweighs the cooling effect of the movement of the rock towards the surface. The Mg rim composition of garnet would have slightly increased during heating and then decreased during cooling. We assumed that when the rock cooled back to 800°C at a depth of 11.8 km, the zoning profile of garnet became flat again at the level of the measured core composition (which reflects a temperature of 800°C). Thus, $\int D dt$ was evaluated from the 11.8 km. The cooling rate corresponding to a fixed exhumation velocity varies as a function of depth. For $V_z = 2 \text{ mm/yr}$, it varies from $\sim 50^\circ\text{C}$ at 10 km to $\sim 145^\circ\text{C}$ at 5 km (inset of Fig. 6). Assuming that V_z did not change significantly above 5 km depth, the two stage model developed above suggests that the HHC samples exhumed to the surface from a depth of $\sim 34 \text{ km}$ within $\sim 8 \text{ Ma}$.

Duchêne et al. [29] analyzed the uplift rate of a number of eclogites from different tectonic regimes and found that in each case the exhumation history is characterized by an initial rapid uplift followed by a much slower one, as in the case of the Himalayan metamorphic rocks. This implies that either the uplift rate substantially slowed down with time within a rather small time interval, presumably as a result of tectonic slicing followed by erosion, or that there was a vertical velocity gradient in each case. The latter condition requires [29] that the rocks must have flowed horizontally at shallow depth where the change of V_z took place, since the divergence of velocity of an incompressible material must be zero. It is not possible to distinguish between the two alternatives at this stage, but the repetitive nature of the change of exhumation velocity as a function of depth is intriguing, as also the fact that the HHC samples are bounded on the north by an extensional system (Fig. 1). It, therefore, seems likely that a part of the change of exhumation rate might have been accommodated by extension throughout the HHC.

Acknowledgements

Thanks are due to Dr. Stephanie Duchêne and Professor Linc Hollister for their constructive reviews of the manuscript, and to Max Tirone for

his help with the computer programming. We also thank Mr. M. Fukuoka and Mr. N.C. Pant for help with the microprobe analyses at the initial stages of this work. This research was supported by an NSF grant EAR 9805232, a joint grant from the NSF International Program, INT 0002004, and the DST, Government of India, DST/INT/US(NSF-RP031)/2000, and a field grant from the Centre for Advanced Studies, Department of Geological Sciences, Jadavpur University. [FA]

References

- [1] K.V. Hodges, The thermodynamics of Himalayan orogenesis, in: P.J. Treloar, P.J. O'Brien (Eds.), *What drives Metamorphism and Metamorphic Reactions?*, Geol. Soc., London, 1998, pp. 7–22.
- [2] M.T. Harrison, F.J. Ryerson, P. Le Fort, A. Yin, O.M. Lovera, E.J. Catlos, A late Miocene–Pliocene origin for the Central Himalayan inverted metamorphism, *Earth Planet. Sci. Lett.* 146 (1997) E1–E7.
- [3] P.K. Zeitler, N.M. Johnson, C.W. Naeser, R.A.K. Tahir-kheli, Fission track evidence for Quaternary uplift of the Nanga Parbat region, Pakistan, *Nature* 300 (1982) 255–257.
- [4] J-P. Burg, P. Davy, P. Nievergelt, F. Oberli, D. Seward, Z. Diao, M. Meier, Exhumation during crustal folding in the Namche-Barwa syntaxis, *Terra Nova* 9 (1997) 53–56.
- [5] A. Lasaga, Geospeedometry: an extension of geothermometry, in: S.K. Saxena (Ed.), *Kinetics and Equilibrium in Mineral Reactions*, *Advances in Physical Geochemistry*, vol. 2, Springer, New York, 1983, pp. 81–114.
- [6] S. Neogi, M. Dasgupta, M. Fukuoka, High P – T metamorphism, dehydration melting, and generation of migmatites and granites in the higher Himalayan crystalline complex, Sikkim, India, *J. Petrol.* 39 (1998) 61–99.
- [7] W. Carlson, C. Denison, Mechanisms of porphyroblast crystallization: results from high-resolution computed X-ray tomography, *Science* 257 (1992) 1236–1239.
- [8] J. Ganguly, S.K. Saxena, *Mixtures and Mineral Reactions*, Springer, Berlin, 1987.
- [9] J. Ganguly, W. Cheng, M. Tirone, Thermodynamics of aluminosilicate garnet solid solution: new experimental data, an optimized model, and thermometric applications, *Contrib. Miner. Petrol.* 126 (1996) 137–151.
- [10] R. Lindstrom, M. Viitanen, J. Juhanoja, P. Hölttä, Geospeedometry of metamorphic rocks: examples in the Rantasalmi-Sulkava and Kiuruvesi areas, eastern Finland. Biotite-garnet diffusion couples, *J. Metamorph. Geol.* 9 (1991) 181–190.
- [11] J. Crank, *The Mathematics of Diffusion*, Oxford, 1975.
- [12] J.M. Ferry, F.S. Spear, Experimental calibration of the partitioning of Fe and Mg between biotite and garnet, *Contrib. Miner. Petrol.* 66 (1978) 113–117.
- [13] J. Ganguly, W. Cheng, S. Chakraborty, Cation diffusion in aluminosilicate garnets: experimental determination in pyrope-almandine diffusion couples, *Contrib. Miner. Petrol.* 131 (1998) 171–180.
- [14] J.R. Manning, *Diffusion Kinetics for Atoms in Crystals*, Van Nostrand, Princeton, NJ, 1968.
- [15] F. James, M. Roos, MINUIT, a system for function minimization and analysis of the parameter error and correlations, *Comput. Phys. Commun.* 10 (1975) 343–347, CERN/DD, Int. Rep. 75/20.
- [16] J. Ganguly, H. Yang, S. Ghose, Thermal history of mesosiderites: quantitative constraints from compositional zoning and Fe–Mg ordering in orthopyroxenes, *Geochim. Cosmochim. Acta* 58 (1994) 2711–2723.
- [17] M.L. Fuhrman, D.H. Lindsley, Ternary feldspar modeling and thermometry, *Am. Miner.* 73 (1988) 201–216.
- [18] M.J. Holdaway, Application of new experimental and garnet Margules data to the garnet-biotite geothermometer, *Am. Miner.* 85 (2000) 881–892.
- [19] H.-P. Liermann, J. Ganguly, Orthopyroxene–spinel cosmo-geothermometer: experimental calibrations and applications to meteorites, *Lunar and Planet. Sci. Conf.*, 1999.
- [20] M. Stimpfl, J. Ganguly, G. Molin, Fe^{2+} –Mg order–disorder in orthopyroxene: equilibrium fractionation between the octahedral sites and thermodynamic analysis, *Contrib. Miner. Petrol.* 136 (1999) 297–309.
- [21] S.R. Bohlen, W.A. Dollase, V.J. Wall, Calibration and application of spinel equilibria in the system FeO – Al_2O_3 – SiO_2 , *J. Petrol.* 27 (1986) 1025–1034.
- [22] S.K. Saxena, N. Chatterjee, Y. Fei, G. Shen, *Thermodynamic Data on Oxides and Silicates*, Springer, Berlin, 1993.
- [23] J. Ganguly, R.N. Singh, D.V. Ramana, Thermal perturbation during charnockitization and granulite facies metamorphism in southern India, *J. Metamorph. Geol.* 13 (1995) 419–430.
- [24] H.S. Carslaw, J.C. Jaeger, *Heat Conduction of Solids*, 2nd edn., Clarendon Press, Oxford, 1959.
- [25] L. Mercier, J.M. Lardeaux, P. Davy, On the tectonic significance of retrograde P – T – t paths in eclogites of the French massif central, *Tectonics* 10 (1991) 131–140.
- [26] P.C. England, A.B. Thompson, Pressure–temperature–time paths of regional metamorphism. I. Heat transfer during the evolution of regions of thickened continental crust, *J. Petrol.* 25 (1984) 894–928.
- [27] P. England, P. LeFort, P. Molnar, A. Pécher, Heat sources for tertiary metamorphism and anatexis in the Annapurna-Manaslu region, central Nepal, *J. Geophys. Res.* 97 (1992) 2107–2128.
- [28] M.L. Gupta, A. Sunder, S.R. Sharma, Heat flow and heat generation in the Archean Dharwar cratons and implications for the Southern Indian shield geotherm and lithosphere thickness, *Tectonophysics* 194 (1991) 107–122.
- [29] S. Duchêne, J.-M. Lardeaux, F. Albarède, Exhumation of eclogites insights from depth–time path analysis, *Tectonophysics* 280 (1997) 125–140.